A statistical arteriovenous cerebral atlas

A. Dufour* [a,b], O. Tankyevych[c], H. Talbot[d], C. Ronse[a], J. Baruthio[b], and N. Passat[a]

(a) Université de Strasbourg, LSIIT, UMR CNRS 7005, France
(b) Université de Strasbourg, LINC, UMR CNRS 7237, France
(c) Télécom ParisTech, LTCI, UMR CNRS 5141, France
(d) Université Paris-Est, LIGM, UMR 8049 CNRS, France
alice.dufour@unistra.fr

Abstract. In this paper, we propose a pipeline for building statistical cerebrovascular atlases from 3D angiographic datasets. This pipeline relies on recent advances in vessel segmentation and filtering, image skeletonization, and image registration. The generated atlases embed information on vesselness probability, vein/artery discrimination, vessel size and relative orientation. It improves on previously proposed approaches. Experiments performed on a dataset of 54 MRA/MRI images allowed us to propose an original vascular atlas of the whole intracranial volume.

Key words: Vascular atlas, vessel analysis, magnetic resonance angiography.

1 Introduction

The availability of accurate knowledge related to anatomical structures is essential in nearly all the fields of medical image analysis. In the case of vascular networks, such knowledge can be classified into three categories: (*i*) *morphological* (*e.g.*, shape, size, orientation), (*ii*) *structural* (*e.g.*, topology, position, spatial relations), and (*iii*) *functional*. We focus here on the first two categories, which have not been the object of much work since the end of the 80's.

Recent studies, often devoted to the cerebrovasculature, were intended to model information related to potentially complex vascular networks. This complexity arises from the structure of these networks, the wide variety (size, veins/arteries) of the visualized vessels, the image modalities (often non-injected, especially in magnetic resonance angiography –MRA– data), and also from the anatomical variability of the vessels. In this context, the design of no longer deterministic, but *statistical* atlases has been considered. Among other possible applications, such atlases can be of use in the initialization and guidance of automated vessel segmentation and labelling procedures, often important steps in many medical image analysis applications.

This article is organized as follows. Section 2 proposes a state of the art on vascular atlases. Section 3 describes the developed atlas generation pipeline. This pipeline is applied to a 54 images dataset, allowing us to produce an atlas as described in Section 4.

* The research leading to these results has been partially funded by a PhD grant of the *Région Alsace* (France) and the *Centre National de la Recherche Scientifique* (CNRS, France).

2 Previous works

In contrast to other anatomical structures, vascular networks have been infrequently considered for atlas generation. This section proposes a short survey on this research field, mostly focused on cerebrovascular and cardiovascular networks. The reader may find a more complete and up-to-date, state of the art in [18].

Pioneering works and deterministic atlases. The first (hand-made) vascular atlas generated from angiographic data [6], consisted of a (piecewise linear) skeleton modelling the main coronary arteries, providing information on vessel position and trajectory. Since then, other (deterministic) atlases have been proposed.

Early works, based on graphs, focused on symbolic descriptions of vessels (independently from their 3D embedding). The extraction of such graphs has been a frequent application to the first 3D segmentation methods [19]. To avoid segmentation errors, another solution was to consider realistic and easy to process anatomical phantoms [3].

Later works aimed at defining anatomically realistic vascular models. In [13], a geometric atlas of the cerebrovascular network was proposed. Its generation, based on a time of flight –TOF– MRA of a healthy patient, leads to an accurate vascular atlas providing information on the type of vessels (arteries or veins), their position, name, size and topology. Such an atlas, while essentially designed manually, is yet strongly linked to the involved patient image. In [10], a geometric atlas is proposed for coronary arteries. It was created (at least partially) using the vascular information provided by 3D computed tomography angiography –CTA– data of several patients.

Statistical atlases. Non-deterministic, and especially statistical, atlases aim at modelling both invariant information and inter-individual variability among a set of patients, in a unified framework.

In simple cases, for instance when only one vessel has to be modelled, a straightforward strategy consists of creating a shape model. This can be done by computing the mean (fuzzy) image of segmented data, as proposed in [11] for the portal vein entry.

In more complex cases, in particular for whole vascular networks, it becomes necessary to develop strategies for fusing several vascular images. In [4], segmented networks are registered onto a chosen set, considered as the anatomical reference. The computed mean and variance images of distance maps provide a kind of probabilistic atlas. A similar alternative technique is proposed in [5], where the registration process also involves morphological (T2 MRI) data. In some cases, morphological information can be directly obtained from angiographic data, as in [16], where CTA images are considered.

These statistical atlases are essentially devoted to vascular density modelling. In [14] a way to design richer (cerebro)vascular atlases is proposed. Such atlases have the advantage to model not only vascular density, but also information on vessel size and orientation. Despite these improvements, the generation pipeline proposed in [14] presents some weaknesses: (*i*) no vein/artery discrimination, (*ii*) absolute orientations instead of relative ones, (*iii*) use of one specific patient morphology as anatomical reference, and (*iv*) use of binary (segmented) images for size and orientation determination (with possible segmentation errors).

Based on recent advances in (medical and non-medical) image processing, we propose a new pipeline, inspired from the one of [14], that provides solutions to all the weaknesses listed above.

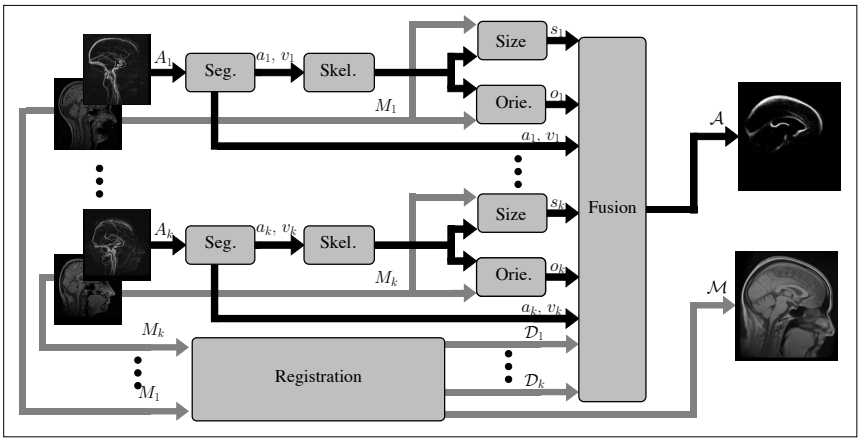

Fig. 1. Atlas generation pipeline. The grey boxes correspond to the steps described in Sec. 3. Seg.: segmentation (Sec. 3.3), Skel.: centerline computation (Sec. 3.4), Size: size computation (Sec. 3.5), Orie.: orientation computation (Sec. 3.5), Registration (Sec. 3.6), Fusion (Sec. 3.7).

3 Atlas generation pipeline

3.1 Input/output

The pipeline takes as input a set $\{(M_i, A_i)\}_{i=1}^{k}$ of $k \in \mathbb{N}$ angiographic images of intracranial volumes. These images need not be similar in terms of modalities and/or acquisition devices, including MRA and/or CTA. It is however mandatory, for each angiographic image $A_i : E \to V$ (E is the 3D brain volume, V is the grey-levels value space), to be associated to a morphological one, $M_i : E \to V$ (*e.g.*, a T1 MRI). This requirement (see Section 3.6) is not actually a problem since such morphological images are generally acquired in addition to both MRA and CTA.

The pipeline provides as output a vascular arteriovenous cerebral atlas modelling statistical information. It fuses, in a unified anatomical reference, several pieces of knowledge related to vascular probability density, vein/artery discrimination, vessels size and relative orientation. This atlas is represented by a pair of images $(\mathcal{M}, \mathcal{A})$. The image $\mathcal{M} : E \to V$ is a (scalar) mean morphological image obtained from the morphologies of the k patients (similar, *e.g.*, to a mean T1 MRI). The vascular (vectorial) part of the atlas is defined as

$$\left| \begin{array}{l} \mathcal{A} : E \to [0,1] \times [0,1] \times \mathbb{T} \times (\mathbb{R}^+)^2 \\ \qquad x \mapsto (\delta(x), \alpha(x), \omega(x), \sigma(x)) \end{array} \right. \tag{1}$$

To each point $x \in E$ is associated the 4-uple $(\delta(x), \alpha(x), \omega(x), \sigma(x))$ where: $\delta(x)$ is the vessel presence probability at x; $\alpha(x)$ is the arterial probability (*i.e.*, a vessel at x has a probability $\alpha(x)$ (resp. $1 - \alpha(x)$) to be an artery (resp. a vein)); $\omega(x)$ is a 3D tensor modelling the mean orientation of the vessels at x, and how these orientations are spread around this mean orientation; finally $\sigma(x)$ provides the mean vessel diameter and its standard deviation at x. (Note that $\alpha(x), \omega(x), \sigma(x)$ are relevant only for $\delta(x) \gg 0$.)

3.2 Outline

The pipeline is organized as illustrated in Fig. 1. The k angiographic images are first segmented, in order to extract both venous and arterial structures (Section 3.3). This is done interactively to lessen segmentation errors. From these binary data, vessel centerlines are extracted (Section 3.4). They provide the relevant *loci* where a multiscale Hessian-based analysis is applied to determine the vessels orientation and size (Section 3.5). Both are computed from the grey-level images (more informative and reliable than the segmented ones). In parallel to these steps, registration is performed between the k morphological images (Section 3.6). This provides $\mathcal{M}$ and the deformation fields associated to the k images. These deformation fields and the knowledge elements are finally combined to define the vascular atlas $\mathcal{A}$ (Section 3.7).

3.3 Vein/artery segmentation

The segmentation step is crucial since (*i*) the vascular density δ is computed as a mean value of the segmented vascular volumes, and (*ii*) the vessel centerlines is computed as their medial axes. It is then important to ensure that there are no false positives, and a minimal amount of false negatives. To avoid post-processing result corrections, we propose to rely on a new interactive segmentation technique [7] coupled with a filtering strategy [17] featuring increased robustness to vessel disconnections. This technique allows the user to choose, in real-time, the best segmentation among a set of preprocessed ones. Moreover, this example-based methodology enables us to perform discriminant segmentation of arteries and veins, thus providing, for each one of the k images, distinct arterial and venous volumes $a_i, v_i \subseteq E$ ($i \in [1, k]$).

3.4 Vessel centerlines computation

The binary volumes a_i, v_i are then skeletonized, to determine the positions of the vessel axes. Contrary to [14], these axes are not directly used to compute the vessels orientation (from the skeleton) and size (from both the skeleton and the binary volumes). They only provide the *loci* where a Hessian-based analysis has to be performed from the images A_i to determine these geometric information. It is then crucial for the computed axes (*i*) to be (globally) centered, and (*ii*) to provide a topologically sound model of the vessel branches. To satisfy these requirements, the algorithm proposed in [1] is applied. It provides skeletonized images $a_i^s, v_i^s \subset a_i, v_i$, without irrelevant branches. The skeleton regularity (not guaranteed here) is desirable but actually not essential, since a confidence neighbourhood is obtained by binary dilation of the skeleton.

3.5 Orientation and size computation

The purpose of this step is twofold. It consists of determining (*i*) the size of the vessels and (*ii*) their orientation. Hessian-based analysis constitutes a standard approach for vessel filtering, as it provides a model of the second order differential properties of the image, as well as size, orientation and characterization of several geometric structures. Based on *ad hoc* "vesselness" functions [15, 8], it is in particular possible to determine

the orientation of vessels in A_i images. Note that the restriction of this study to the a_i^s, v_i^s parts of A_i allows us to reduce the computational cost and to avoid possibly erroneous results away from the vessel axes. The computation of a vesselness measure is done in a multiscale fashion [9]. The scale for which the response is maximal in $x \in E$ corresponds to a convolution kernel directly correlated to the size of the vessel visualised in x. The principal orientation (first eigenvector of the Hessian matrix) at x for this scale is then the vessel orientation. This strategy provides orientation $o_i(x) \in \mathbb{R}^3$ and size $s_i(x) \in \mathbb{R}^+$ information for any point $x \in a_i^s \cup v_i^s$. It is however mandatory to extend these information to the whole vascular volume A_i. For $s_i(.)$, this can be done by performing in each $x \in a_i^s \cup v_i^s$ a variant flat dilation by a spherical structuring element whose radius is determined by $s_i(x)$ (the grey-level values correspond to s_i). For $o_i(.)$, which is no longer a scalar function, but a vectorial one, this can be done by computing, for each $x \in A_i$, a weighted average value of the orientations $o_i(y)$ of the points y located in the intersection of a_i^s, v_i^s and a neighbourhood of x. For each image A_i, this step outputs a size function $s_i : a_i \cup v_i \to \mathbb{R}^+$ and an orientation function $o_i : a_i \cup v_i \to \mathbb{R}^3$.

3.6 Registration

Registration is necessary to estimate the deformation fields $\mathcal{D}_i : E \to E$, enabling us to map the information of any data (M_i, A_i) onto a common anatomical reference. These fields are estimated from the (morphological) M_i data, using a groupwise nonrigid registration technique [12]. In comparison to [14], this eschews the possible anatomical bias induced by the use of a specific image M_i as reference. Once the $\mathcal{D}_i$ fields are known, the anatomical reference $\mathcal{M}$ can be computed as the mean value of the k registered M_i images, *i.e.*, as $\mathcal{M} = \frac{1}{k}\sum_{i=1}^{k} \mathcal{D}_i^{-1} \circ M_i$. Note that the $\mathcal{D}_i$ fields provide translation information, making it possible to put in correspondence some scalar information (*i.e.*, a_i, v_i, s_i) of A_i at x, and of $\mathcal{A}$ at $\mathcal{D}_i(x)$. Note, moreover, that it also provides rotation information between x and $\mathcal{D}_i(x)$, enabling us in particular to conveniently register the orientations $o_i(.)$, thus leading to relative orientations $\omega(.)$ in $\mathcal{A}$, *i.e.*, vessel orientations correlated to the neighbouring (registered) morphological structures (*vs*. absolute orientations in [14]).

3.7 Knowledge fusion

For each data (M_i, A_i), we then have vascular volumes a_i, v_i, orientations o_i, sizes s_i, and a deformation field $\mathcal{D}_i$. We can now compute $\mathcal{A}$. The field δ is defined as the mean value of the vascular volumes $a_i \cup v_i$, *i.e.*, $\delta(x) = \frac{1}{k}\sum_{i=1}^{k} |\mathcal{D}_i^{-1}(x) \cap (a_i \cup v_i)|$, while α is expressed as the arterial ratio in δ, *i.e.*, $\alpha(x) = \frac{1}{\delta(x)}\sum_{i=1}^{k} |\mathcal{D}_i^{-1}(x) \cap a_i|$ whenever $\delta(x) > 0$. Similarly to δ, σ is defined by the mean value of the sizes s_i, *i.e.*, $\sigma(x) = \frac{1}{\delta(x)}\sum_{i=1}^{k} s_i \circ \mathcal{D}_i^{-1}(x)$, enriched by the associated standard deviation (not formalized here due to lack of space). Finally, the orientation ω is computed as a tensor. Based on the covariance matrix induced by the k registered (normalised) vectors $o_i(\mathcal{D}_i(x))$, the vessel orientation at x is computed as the first eigenvector of the matrix, while the second and third eigenvectors and eigenvalues provide the geometric spread of this orientation in the normal plane. Finally, the proposed pipeline then provides an atlas $\mathcal{A}$ compliant with the one expressed in Formula (1).

4 Experiments and results

Material. The proposed pipeline was used to generate a cerebrovascular atlas from a dataset of phase contrast (PC) MRA images. Each data is composed of a phase (angiographic, A_i) and a magnitude (morphological, M_i) image. In these first experiments, we chose to consider data similar to those of [14] (i.e. non injected, millimetric resolution), in order to facilitate qualitative and quantitative comparisons (which will be fully presented in an extended version of this work). Further experiments will also involve heterogeneous (CTA, MRA), submillimetric, and injected data, with the purpose of generating a more accurate atlas than this preliminary one.

Computational cost. The process is fully automatic, except the interactive part of the segmentation method [7], which requires only a few seconds per image. The most time-consuming step remains the (submillimetric resolution) groupwise nonrigid registration [12], which requires approximately 3 to 4 hours per image. This registration step, which can be performed in parallel to all the other ones (except the –final– fusion step, which requires a few minutes), defines a lower bound for the time cost of the pipeline. Note that new images can be further added to an atlas already generated, progressively enriching it without the necessity to recompute all the deformation fields.

Results. Due to the quasi-automation of the process, large datasets can be considered for atlas generation. In these experiments, 54 image couples (M_i, A_i) were processed (*vs*. 18 in [14], due to manual validations and corrections of the segmented results). The obtained atlas is partially illustrated in Figs. 2 and 3.

Some (partial) quantitative information on this atlas are illustrated in Fig. 4. Fig. 4(a) (resp. Fig. 4(b)) provides the histogram of δ (resp. of the mean part of σ), *i.e*., the vascular probability distribution (resp. the mean size distribution) over the vascular volume of E, *i.e*., $\delta^{-1}(]0, 1])$. Note that these two histograms are not directly comparable to [14] (Tabs. 1 and 2), where the computation was made on the whole head, *vs*. the intracranial volume, here. Also note that in [14] (Tab. 3), more that 70% of the vascular volume did not present a significative orientation (due to standard deviations higher than $\pi/4$ in spherical coordinates. The use of relative instead of absolute orientations should makes it possible to improve this score.

5 Conclusion

A cerebrovascular atlas generation pipeline was proposed. This is a challenging problem, and our solution provides improved results in comparison to previous approaches.

Further works will include more extensive and quantitative analysis of these improvements, in particular in comparison to [14]. We also plan to introduce some information on anatomical relations in the proposed cerebrovascular atlases, in particular between vessels and the main neighbouring morphological structures (skull, brain structures, etc.) [2]. This approach, that presents similarities with the one proposed in [10]) in the context of cardiac vessels, will require processing both angiographic and morphological (*i.e*., both CT/MRI and CTA/MRA) data in a unified way.

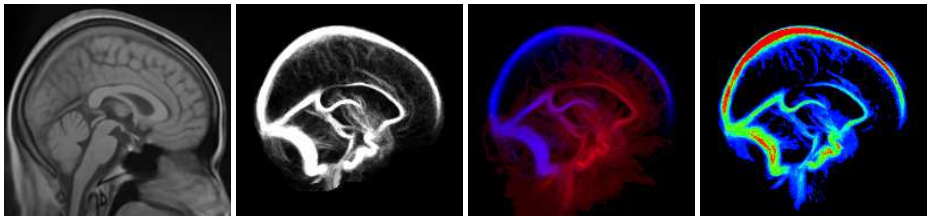

(a) (b) (c) (d)

Fig. 2. Atlas generated from 54 images (2D views). (a) Anatomical reference $\mathcal{M}$ (sagittal medial plane). (b–d) Vascular image $\mathcal{A}$. (b) Vascular density δ, from black (0) to white (1). (c) Vein/artery density α, from blue (0, veins only) to red (1, arteries only). (d) Vessel diameters σ (mean value only), from blue ($\leq$ 0.5mm) to red ($\geq$ 5mm). (b–d) are viewed as maximal intensity projections (sagittal plane).

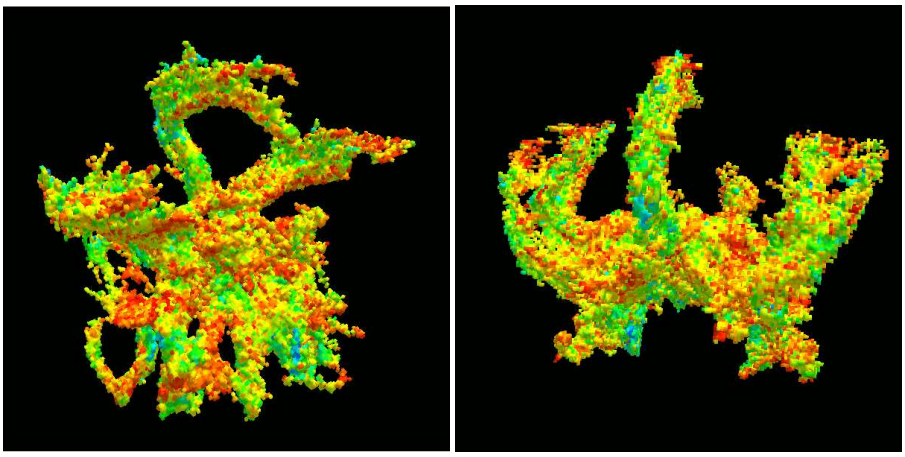

(a) (b)

Fig. 3. Arteriovenous atlas generated from 54 images (3D views). Vessel orientations ω (inclination component $\theta \in [0, \pi/2]$ of the mean orientation, in a spherical coordinate system), from blue (vertical, $\theta = 0$) to red (horizontal, $\theta = \pi/2$). (a,b) two views restricted to arteries.

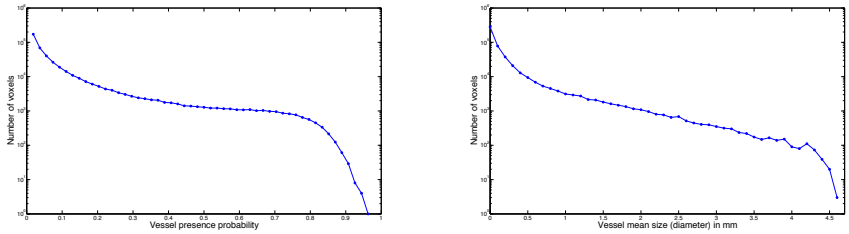

(a) (b)

Fig. 4. Vessel probability and size distribution over the vascular volume $\delta^{-1}(]0, 1])$ of $\mathcal{A}$ (see Fig. 2). (a) Probability (δ) histogram. (b) Mean size (part of σ) histogram.

References

1. Bertrand, G., Couprie, M.: A new 3D parallel thinning scheme based on critical kernels. In: DGCI. LNCS, vol. 4245, pp. 580–591. Springer (2006)
2. Bloch, I.: Fuzzy spatial relationships for image processing and interpretation: a review. Image and Vision Computing 23(2), 89–110 (2005)
3. Chalopin, C., Finet, G., Magnin, I.E.: Modeling the 3D coronary tree for labeling purposes. Medical Image Analysis 5(4), 301–315 (2001)
4. Chillet, D., Jomier, J., Cool, D., Aylward, S.: Vascular atlas formation using a vessel-to-image affine registration method. In: MICCAI. LNCS, vol. 2878, pp. 335–342. Springer (2003)
5. Cool, D., Chillet, D., Guyon, J.P., Foskey, M., Aylward, S.: Tissue-based affine registration of brain images to form a vascular density atlas. In: MICCAI. LNCS, vol. 2879, pp. 9–15. Springer (2003)
6. Dodge Jr., J.T., Brown, B.G., Bolson, E.L., Dodge, H.T.: Intrathoracic spatial location of specified coronary segments on the normal human heart. Circulation 78(5), 1167–1180 (1988)
7. Dufour, A., Passat, N., Naegel, B., Baruthio, J.: Interactive 3D brain vessel segmentation from an example. In: ISBI. pp. 1121–1124. IEEE (2011)
8. Frangi, A.F., Niessen, W.J., Hoogeveen, R.M., van Walsum, T., Viergever, M.A.: Model-based quantitation of 3-D magnetic resonance angiographic images. IEEE Transactions on Medical Imaging 18(10), 946–956 (1999)
9. Lindeberg, T.: Edge detection and ridge detection with automatic scale selection. In: CVPR. pp. 465–470. IEEE (1996)
10. Lorenz, C., von Berg, J.: A comprehensive shape model of the heart. Medical Image Analysis 10(4), 657–670 (2006)
11. Naegel, B., Ronse, C., Soler, L.: Using grey-scale hit-or-miss transform for segmenting the portal network of the liver. In: ISMM. Computational Imaging and Vision, vol. 30, pp. 429–440. Springer SBM (2005)
12. Noblet, V., Heinrich, C., Heitz, F., Armspach, J.P.: Symmetric nonrigid image registration. application to average brain templates construction. In: MICCAI. LNCS, vol. 5242, pp. 897–904. Springer (2008)
13. Nowinski, W., Volkau, I., Marchenko, Y., Thirunavuukarasuu, A., Ng, T., Runge, V.: A 3D model of human cerebrovasculature derived from 3T magnetic resonance angiography. NeuroInformatics 7(1), 23–36 (2009)
14. Passat, N., Ronse, C., Baruthio, J., Armspach, J.P., Maillot, C.: Magnetic resonance angiography: From anatomical knowledge modeling to vessel segmentation. Medical Image Analysis 10(2), 259–274 (2006)
15. Sato, Y., Nakajima, S., Shiraga, N., Atsumi, H., Yoshida, S., Koller, T., Gerig, G., Kikinis, R.: Three-dimensional multi-scale line filter for segmentation and visualization of curvilinear structures in medical images. Medical Image Analysis 2(2), 143–168 (1998)
16. Shahzad, R., Schaap, M., van Walsum, T., Klien, S., Weustink, A.C., van Vliet, L.J., Niessen, W.J.: A patient-specific coronary density estimate. In: ISBI. pp. 9–12. IEEE (2010)
17. Tankyevych, O., Talbot, H., Dokládal, P., Passat, N.: Direction-adaptive grey-level morphology. Application to 3D vascular brain imaging. In: ICIP. pp. 2261–2264. IEEE (2009)
18. Tankyevych, O., Talbot, H., Passat, N., Musacchio, M., Lagneau, M.: Angiographic image analysis. In: Dougherty, G. (ed.) Medical Image Processing: Techniques and Applications (Ch. 6). Springer (2011)
19. Zahlten, C., Jürgens, H., Evertsz, C.J.G., Leppek, R., Peitgen, H.O., Klose, K.J.: Portal vein reconstruction based on topology. European Journal of Radiology 19(2), 96–100 (1995)